14th International Symposium on Turbulence and Shear Flow Phenomena (TSFP14)
Heidelberg, Germany, July 28–31, 2026

REDUCED-ORDER MODEL FOR FLOW DYNAMICS AND INTER-SCALE ENERGY TRANSFER IN THIN FLAT PLATE WAKES

Xinyang Liu
Department of Mathematics and Statistics
University of Calgary
2500 University Dr. NW, Calgary, AB T2N 1N4
xinyang.liu@calgary.ca

Robert J. Martinuzzi
Department of Mechanical and Manufacturing Engineering
University of Calgary
2500 University Dr. NW, Calgary, AB T2N 1N4
rmartinu@ucalgary.ca

Chris Morton
Department of Mechanical Engineering
McMaster University
1280 Main St W, Hamilton, ON L8S 4L8
mortoc5@mcmaster.ca

Wenyuan Liao
Department of Mathematics and Statistics
University of Calgary
2500 University Dr. NW, Calgary, AB T2N 1N4
wliao@ucalgary.ca

ABSTRACT

A reduced-order model (ROM) is developed for the flow over a thin flat plate normal to a uniform stream at a Reynolds number (*Re*) of 400 to investigate coherent flow dynamics and inter-scale energy transfer. The ROM is developed from a direct numerical simulation (DNS) dataset. The wake is fully turbulent and the coherent motions comprise the primary periodic vortex shedding instability as well as secondary instabilities associated with breathing/flapping and rib-like streamwise vortex braids between the primary roller vortices. These coherent motions are captured using nine finite-impulse response spectral proper orthogonal decomposition (FIR-SPOD) modes. A low-dimensional nonlinear dynamical system governing their temporal evolution is identified from Galerkin projection of the Navier–Stokes momentum equations onto the FIR-SPOD bases. The contribution of the truncated modes to the flow dynamics, including the dissipation and the Reynold stress, is modelled as diffusion based on the resolved modes using eddy viscosity. The eddy viscosity is modeled as a function of the instantaneous kinetic energy optimized by minimizing the energy difference between the FIR-SPOD modes and the Galerkin system solutions using the adjoint method. The solutions of the reconstructed ROM are shown to capture the observed FIR-SPOD modes dynamics, which enables the investigation of the energy transfer through the nonlinear coefficients in the ROM.

INTRODUCTION

Flow instabilities over a thin flat plate differ from those over elliptical and circular cylinders (Thompson *et al.*, 2014; Williamson, 1996), despite the thin flat plate being a special case of the degenerate elliptical cylinder. The wake reaches a fully turbulent state at a Reynolds number (*Re*) of 400 in the thin flat plate. The rib-like streamwise vortices emerge at a lower *Re* ($Re \sim 105$) than for the circular cylinders ($Re \sim 180$), perturbing the primary vortices developed due to the Hopf bifurcation (Thompson *et al.*, 2014). Also, unlike the flow over the circular cylinder, the flow over the thin flat plate contains an additional low-frequency instability giving rise to a shear flapping motion in addition to the slow-varying motion documented by Noack *et al.* (2003). This study focuses on the flow over a thin flat plate and aims to build an interpretable low-dimensional framework for investigating the mechanisms and energy transfer between modes and their impact on the flow dynamics. Unlike the circular cylinder wake, the thin flat plate wake exhibits a more complex energy transfer pathway due to the additional low-frequency instabilities. Moreover, this can explain why the flow over a thin flat plate reaches a fully-turbulent state at a much lower *Re*.

Motions of different scales interact nonlinearly to transfer energy to smaller scales and generate Reynolds stresses (Tennekes & Lumley, 1972). Energy is primarily generated through the deformation of the large scales and dissipated at the smallest Kolmogorov scales. In the inertial scale, the energy is transferred down to a smaller scale almost without loss. Effectively, the energy is redistributed in the frequency and wavenumber spectrum, producing the Reynolds stresses which in turn contribute to the deformation of large-scale eddies, thereby the turbulent production. Modeling the small scale allows an effective description of flow dynamics in terms of large-scale coherent motions.

Reduced-order modeling (ROM) preserves the essential features and properties of the flow, and reduces the complexity of the dynamical system reconstruction by resolving the energy-producing scales and modeling the transfer to the inertial scales. In this work, we reduce the complexity of ROM while preserving the interpretability of the ROM by selecting a small number of energetic modes representing the flow instabilities individually and capturing the large-scale motion collectively.

The first step in formulating a ROM is to identify a suitable low-dimensional space that captures the flow dynamics. Proper orthogonal decomposition (POD) is commonly used to obtain an energy-ranked orthogonal basis for the velocity field $\mathbf{u}(\mathbf{x},t)$ by extracting the flow's coherent temporal-spatial structure (Aubry *et al.*, 1988; Berkooz *et al.*, 1993). Finite impulse response-based spectral proper orthogonal decomposition (FIR-SPOD), as an extension of POD, separates the uncorrelated spectral contributions at different frequencies embedded within the modes. The separated energy is redistributed to other modes, leading to a clearer interpretation of coherent motion than POD (Sieber *et al.*, 2016). Spectral proper orthogonal decomposition (SPOD) and the discrete Fourier transform

(DFT), as spectrally pure decomposition techniques, lose information characterizing the broadband phenomena (Towne *et al.*, 2018). FIR-SPOD is a compromise, keeping the benefits of both approaches to produce more physically interpretable modes with a continuous spectrum.

Here, a dynamical system of nonlinear ordinary differential equations (nODE) is identified by projecting the Navier-Stokes equations on the basis consisting of nine FIR-SPOD modes. The six most energetic modes that capture the large-scale motion and exhibit a recognizable pattern are first selected. The other three modes are those showing a strong quadratic correlation with the previous six modes, implying a nonlinear contribution to the coherent motion. The underlying physical mechanism of nonlinear interactions among scales in the energy cascade cycle can be further uncovered with the reconstructed system (Holmes *et al.*, 1996). Equation closure is achieved by modeling the unresolved Reynolds stresses and dissipation following the Heisenberg model through the eddy viscosity, which can be optimized by adjoint methods (Aubry *et al.*, 1988; Protas *et al.*, 2015). The adjoint method avoids the computation of the implicit derivative of state variables with respect to the eddy viscosity by introducing an extra adjoint variable. The adjoint equation governing the adjoint state variable assesses the sensitivity of the Galerkin system as well (Plessix, 2006).

The objective of this study is to better understand the interactions between the flow instabilities through the development of a nonlinear system identification framework. The energy transfer through the nonlinear interaction within one or between different scales of motion can be further investigated. Although the nonlinear terms in the reconstructed dynamical system are often neglected due to the dominance of the linear terms over the phase-space trajectory, recovering and investigating the nonlinear terms is still essential for understanding the effect of the triadic interaction on the redistribution of energy within the wavenumber and frequency spectrum, underlying the production of Reynolds stress.

Flow Dataset Description

The dataset used to construct the reduced-order model is from DNS using Nektar++ (Rosin, 2025). The dataset contains the velocity field (u, v, w) and a full pressure field (p). Simulations are conducted for 200 periodic shedding cycles and sampled at a rate of approximately 20 snapshots per shedding cycle with a vortex shedding frequency $f_{vs} \sim 0.152$. The dataset is defined on the interrogation window spatially, which is a sub-domain of the simulation space, capturing the wake formation region. Figure 1 shows a setup schematic at the 2D plane $z = 0$. The interrogation window is displayed in red.

The thin flat plate is spanwise homogeneous and emulates an infinite span by imposing the periodic boundary condition on the spanwise ends, with a spanwise length $s = 10d$. It has been verified against experiments that the flow reaches a fully turbulent state at a low $Re = 400$. The spatial resolution of the data significantly exceeds the number of snapshots, leading to the choice of snapshot-based decomposition technique.

METHODOLOGY

Suppose that the raw velocity field is defined as the vector $\mathbf{u}(\mathbf{x}, t) \in \Omega \times [0, T]$ and the data are in the matrix form $\mathbf{u} \in \mathscr{M}_{(n_s \times n_c) \times n_t}$, where n_s, n_t and n_c denote the dimensions of the space, time and velocity components and $n_s \times n_c \gg n_t$. The velocity is firstly divided into the mean field $\mathbf{U}$ and the fluctuation vector $\mathbf{u}'$ by Reynolds decomposition. The total kinetic energy (TKE) of fluctuation is calculated as the temporal average of the spatial inner product of the fluctuation with itself, TKE $= \frac{1}{2}\overline{\langle \mathbf{u}', \mathbf{u}' \rangle_\Omega}$.

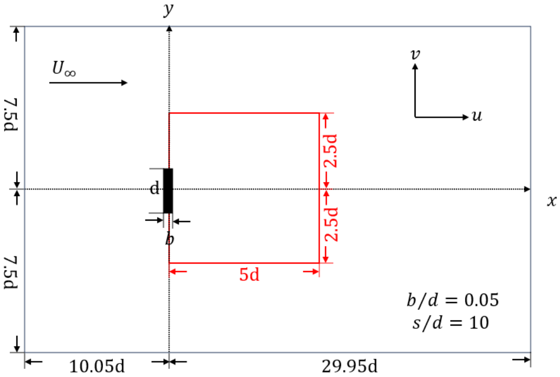

Figure 1: Schematic of geometry and nomenclature for thin flat plate in uniform flow over the 2D plane $(z = 0)$

The Dimension Reduction (FIR-SPOD)

In FIR-SPOD, a filter $\{g_k\}_{k=-N_f}^{N_f}$ is applied to each element of the temporal covariance matrix of fluctuation along the diagonal, where a periodic boundary is assumed on the covariance matrix when filtering. Ideally, the filter size N_f is chosen to be the characteristic time scales of the flow, or a time span where the coherent structure shows constant dynamics if known. Each element of the filtered temporal covariance matrix of fluctuation $\mathbf{R} \in \mathscr{M}_{(n_t \times n_t)}$ can be written as:

$$R_{ij} = \frac{1}{n_t} \sum_{k=-N_f}^{N_f} g_k \langle \mathbf{u}'(\mathbf{x}, t_{i+k}), \mathbf{u}'(\mathbf{x}, t_{j+k}) \rangle_\Omega. \quad (1)$$

The FIR-SPOD temporal modes a_i are obtained as eigenvectors from the eigendecomposition of $\mathbf{R}$. The spatial modes ϕ_i are the projection coefficients of u' onto the space where all the temporal modes a_i compose its orthogonal basis. u' can then be exactly recovered using all the modes: $\mathbf{u}'(\mathbf{x}, t) = \sum_{i=1}^{n_t} \phi_i(\mathbf{x}) a_i(t)$. The spatial mode is normalized $(||\phi_i||^2 = \langle \phi_i, \phi_i \rangle_\Omega = 1)$, and the temporal mode is correspondingly scaled to maintain the reconstruction of $\mathbf{u}'$.

The contribution to the TKE of each FIR-SPOD mode can be calculated using only the temporal coefficients $k_i = \frac{1}{2}\overline{a_i a_i}$. The TKE can be exactly recovered from: TKE $= \sum_{i=1}^{n_t} k_i$. The coherent motion $\mathbf{u}^c$ is approximated by the first N selected modes, where $N << n_t$.

$$\mathbf{u}(\mathbf{x}, t) = \mathbf{U}(\mathbf{x}) + \overbrace{\underbrace{\sum_{i=1}^{N} \phi_i(\mathbf{x}) a_i(t)}_{\approx \mathbf{u}^c} + \underbrace{\sum_{i=N+1}^{n_t} \phi_i(\mathbf{x}) a_i(t)}_{\mathbf{u}''}}^{\mathbf{u}'}. \quad (2)$$

FIR-SPOD bridges the gap between POD and DFT by applying a low-pass filter on the temporal covariance matrix to augment the diagonal similarity (Sieber *et al.*, 2016). The uncorrelated motion may be embedded within the POD modes representing the coherent motion because the basis is not frequency-ranked. Additionally, modes containing coherent structures but with low energy content can be mistakenly truncated. Therefore, to optimize the mode interpretability compared with the POD method, stronger filtering of incoherent motions is essential. Spectral proper orthogonal decomposition (SPOD) and the discrete Fourier transform (DFT) can isolate the dominant frequency within each mode (Towne *et al.*, 2018). However, because the spectra of the broadband phenomena are discretized when computing the cross-spectral density matrix, they often neglect other nearby dominant frequencies which imply energy exchange with coherent motion of different frequencies, leading to a loss of information. FIR-SPOD can not only produce a more interpretable ROM than POD, but also acts as a bandwidth filter centered at the peak frequency on the spectrum of temporal modes. These qualities result in clearer and more physically interpretable modes compared to POD by reducing the variance of amplitude along diagonals on the covariance matrix and redistributing the dynamic content to other modes. Only the modes showing clear spatial and temporal structure (e.g., peak frequency/wavelength) and significant energy contributions are chosen to form the trial space for Galerkin projection in system reconstruction.

The Galerkin Projection

Galerkin projection reduces the complexity of the dynamical system by projecting the governing equations onto a subspace spanned by a finite set of modes. An orthogonal basis, such as POD spatial modes, is preferred in Galerkin projection because orthogonality can further sparsify the dynamical system and simplify the solving process. In this study, the ROM is reconstructed by projecting the Navier-Stokes equation of momentum onto the FIR-SPOD spatial modes. However, the spatial modes $\phi_i(\mathbf{x})$, the projection of $\mathbf{u}'$ on each eigenvector of $\mathbf{R}$, are no longer orthogonal as for POD spatial modes. When the number of the chosen modes N is sufficiently small, the mass matrix $\mathbf{M} \in \mathscr{M}_{N\times N}$ is close to an orthogonal matrix, where each element is defined as

$$M_{rs} = <\phi_r, \phi_s>_\Omega = \int_\Omega \phi_r \phi_s dv, \quad r,s = 1,\ldots,N. \tag{3}$$

$\mathbf{M}$ serves as a weighting matrix of the temporal derivative in the system identification (Noack *et al.*, 2011). The introduction of the mass matrix compensates for the loss of orthogonality in the FIR-SPOD spatial modes and enables the combination of the Galerkin projection with more general modal decomposition methods.

The pressure field is first Reynolds-averaged, and the pressure fluctuations are subsequently modeled using quadratic stochastic estimation (QSE) (Ausseur *et al.*, 2006). Through the pressure-Poisson equation, pressure fluctuation can be fully recovered by quadratic regression of all the temporal modes. Therefore, the pressure fluctuation can be approximated as a quadratic combination of resolved FIR-SPOD modes with coefficients determined through QSE (Noack *et al.*, 2005).

$$p(\mathbf{x},t) = P(\mathbf{x}) + p'(\mathbf{x},t), \tag{4}$$

$$p'(\mathbf{x},t) = \underbrace{\sum_{i,k=0}^{N} p_{ik}(\mathbf{x}) a_i(t) a_k(t)}_{\approx p^c} + \underbrace{\sum_{i>N||k>N}^{n_t} p_{ik}(\mathbf{x}) a_i(t) a_k(t)}_{p''}.$$

After truncating the modes based on energy content and physical interpretation, the equations need to be mathematically stabilized; physically, the Reynolds stress and dissipation, accounting for unresolved parts, need to be modeled. The Heisenberg model suggests that unresolved Reynolds stress is proportional to resolved strain stress (Aubry *et al.*, 1988). Therefore, the convection term including the fluctuation residual, indicating the energy transfer between the truncated microscale and the large-scale coherent motions, can be estimated as the diffusion term through the eddy viscosity ν_T. The reconstructed dynamical system for FIR-SPOD modes $\frac{da_i}{dt} - f_i(\mathbf{a}) = 0, i = 1,\ldots,N$ can be written as:

$$\underbrace{\sum_{j=1}^{N} M_{ji} \frac{da_j}{dt}}_{\frac{da_i}{dt}} = -\langle \nabla P, \phi_i \rangle_\Omega + \left(\frac{1}{Re} + \nu_T(e)\right) \sum_{j=0}^{N} \underbrace{\langle \Delta\phi_j, \phi_i \rangle_\Omega}_{l_{ij}} a_j$$

$$- \sum_{j,k=0}^{N} \underbrace{\langle \left(\phi_j \cdot \nabla\right) \phi_k + \nabla p_{jk}, \phi_i \rangle_\Omega}_{q_{ijk}} a_j a_k. \tag{5}$$

The initial eddy viscosity ν_T° is chosen from Östh *et al.* (2014) and defined as:

$$\nu_T^\circ := \nu_T^a \sqrt{\frac{E(t)}{\tilde{E}}}, \tag{6}$$

which amplifies the dissipation when the instantaneous resolved kinetic energy $E(t)$ by the Galerkin solutions exceeds the resolved TKE $\tilde{E}$ by the chosen FIR-SPOD modes, further guarantees the boundness of the Galerkin solution.

Eddy Viscosity Optimization by The Adjoint Method and Solution of System

Protas *et al.* (2015) proposed to model the eddy viscosity as a functional of instantaneous kinetic energy contained in the chosen modes, denoted by $\nu_T(e), \quad e \in \mathscr{I} = [0, E_{\max}]$ where $E_{\max}$ represents the maximum kinetic energy that the selected FIR-SPOD modes contain. Suppose the eddy viscosity $\nu_T(e)$ is defined on the Hilbert space $L_2(\mathscr{I})$, which contains all square-integrable functions defined on $\mathscr{I}$. $\nu_T(e)$ is optimized to minimize the difference between the kinetic energy of the N FIR-SPOD modes ensemble $\tilde{E}(t)$ and the kinetic energy of the corresponding dynamical system solutions $E(t) = \sum_{i=1}^{N} a_i^2(t)$:

$$\mathscr{L}(\nu_T) = \frac{1}{2T} \int_0^T \left[E(t;\nu_T) - \tilde{E}(t)\right]^2 dt. \tag{7}$$

The adjoint-state method is a preferable choice to compute the gradient of the loss functional. the adjoint methods avoid the computation of $\frac{\partial a_i}{\partial \nu_T}$ as it requires only one extra adjoint equation to solve, whose computation speed is irrelevant to the number of parameters (Plessix, 2006). The system of the adjoint variables $\mathbf{a}^* = \left[0, a_1^*(t), \ldots, a_N^*(t)\right]$ is computed as:

$$-\sum_{j=1}^{N} M_{ij} \frac{da_j^*}{dt} = \sum_{j=1}^{N} A_{ji} a_j^* + \frac{1}{T} \left[E(t;\nu_T) - \tilde{E}(t)\right] a_i \tag{8}$$

$$a_i^*(T) = 0, \quad i = 1,\ldots,N, \tag{9}$$

where $A_{ij} = \sum_{k=0}^{N} (q_{ijk} + q_{ikj}) a_k + (\frac{1}{Re} + \nu_T + \frac{d\nu_T}{de} a_i a_j) l_{ij}$. Thus, the L_2 gradient of loss functional (7) for $e \in [0, E_{max}]$

can be evaluated as

$$\nabla^{L_2}\mathscr{L} = \sum_{E(a(t))=e} \frac{\sum_{i=0,j=0}^{N} l_{ij} a_j(t) a_i^*(t)}{\sum_{i=1}^{N} a_i(t) \sum_{j=1}^{N} M_{ij}^{-1} f_j(\mathbf{a}(t))}. \tag{10}$$

The eddy viscosity is optimized by gradient descent, where the learning rate τ is chosen to minimize the loss function using either gradient-free methods (e.g., Brent's method (Brent, 1973)) or methods with loss functional gradients (e.g., L-BFGS method (Liu & Nocedal, 1989)):

$$\tau = \mathrm{argmin}_{\tau>0}\mathscr{L}(\nu_T - \tau\nabla^{L_2}\mathscr{L}). \tag{11}$$

The equation of kinetic energy of each mode can be computed by multiplying both sides of the reconstructed system with temporal mode and then taking the temporal average. Since $\overline{a_i} = 0, \overline{a_i a_j} = 2k_j\delta_{ij}$, the equation can be simplified to

$$\begin{aligned}\sum_{j=1}^{N} M_{ji}\overline{\frac{da_j}{dt}a_i} = &\sum_{j,k=1}^{n} \underbrace{\langle -\nabla p_{jk}, \phi_i\rangle \overline{a_i a_j a_k} - 2\langle(\nabla p_{0i} + \nabla p_{i0}), \phi_i\rangle k_i}_{\text{pressure diffusion}} \\ &+ \underbrace{\frac{2}{Re}\langle\Delta\phi_i, \phi_i\rangle k_i}_{\text{molecular diffusion}} - \sum_{i,k=1}^{n} \underbrace{\langle(\phi_j\cdot\nabla)\phi_k, \phi_i\rangle\overline{a_i a_j a_k}}_{\text{turbulent diffusion}} \\ &+ \underbrace{\langle(\phi_0\cdot\nabla)\phi_i, \phi_i\rangle k_i}_{\text{advection}} + \underbrace{\langle(\phi_i\cdot\nabla)\phi_0, \phi_i\rangle k_i}_{\text{turbulent production}} \\ &+ \underbrace{\nu_T\left(1 - 2\langle\nabla\phi_i, \nabla\phi_i\rangle\right)k_i}_{\text{dissipation}}.\end{aligned} \tag{12}$$

The triadic interaction $\overline{a_i a_j a_k}$ arises from the terms involving the Reynolds stress and the pressure-velocity coupling in the dynamical system (5). It is weighted by the nonlinear coefficient q_{ijk} in the equation of energy (12). The nonlinear coefficient quantifies the internal energy transfer by the nonlinear interactions arising from the convection and pressure.

RESULTS

FIR-SPOD with a Gaussian filter spanning two shedding cycles is applied on the temporal covariance matrix after the velocity field symmetrization to obtain the antisymmetric, $\{a_i(t), \phi_i^a(\mathbf{x})\}$, and symmetric, $\{s_i(t), \phi_i^s(\mathbf{x})\}$, FIR-SPOD modes. Nine modes are selected to represent coherent motions: first harmonic modes (a_1, a_2) and second harmonic modes (s_2, s_3) with dominant shedding frequency f_{vs} and $2f_{vs}$, shift mode (s_1) contributing to the secondary instability, flapping modes (a_f) potentially relating to the secondary instability, and the induction of the rib-like vortices. The mode s_8 is chosen due to the significant correlation with s_1. The modes a_3, a_4 are selected as a pair showing a mixture of s_1 and a_1, a_2. Mode pairs are selected based on their similar energy content and spectrum but with a $\pi/2$ phase difference (Oberleithner *et al.*, 2011).

Figure 2 shows the aforementioned modes as their spatial functions in planes $z = 0$ and $x = 2$ as well as their frequency spectra. The TKE contribution is measured by the TKE of individual modes over the TKE contained in the interrogation volume. The Reynolds stress $\overline{u'v'}$ contribution is quantified using the techniques in Manohar *et al.* (2023). The first harmonic modes a_1, a_2 contain the most energy (20.8%, 20.49%) and contribution to the Reynolds stress (27.2%, 32.57%), and they have a clear dominant amplitude at f_{vs}. The second harmonic modes s_2, s_3 are also observed with a single peak at $2f_{vs}$.

The shift mode s_1 contributes to the expansion and contraction of the wakes. The process involves energy transfer with the two harmonic pairs. The super-harmonic resonance in the spectrum of s_1 (i.e., a spike at the frequency of second harmonic modes) may imply an energy exchange. The shift mode is nonlinearly correlated with the first harmonic modes that the $s_1 \propto \sqrt{a_1^2 + a_2^2}$ (Noack *et al.*, 2003), which is shown in the paraboloid shape phase diagram in Figure 4.

The flapping mode a_f contributes to the spanwise motion of the wake in the flow-normal direction. This motion has not been observed in the POD of the flow over the circular or square cylinder. a_f may occur from the flapping of the xy plane due to the perturbation of the spanwise inhomogeneous roller, or it records the initialization of the streamwise ribs since the wavelength of eddies of a_f at $x = 2$ falls in the range of the quasi-periodic 3D instability (Thompson *et al.*, 2014).

Mode s_8 has a similar spectrum as s_1 and spatial mode but with a phase shift in wavenumber, which indicates s_8 is related to coherent motion, but it's not clear if s_1 and s_8 are a mode pair because of the significant energy content difference. Modes a_3, a_4 describe a convective motion propagating downstream, similar to the first harmonic modes. The peak of their spectrum is between the low-frequency and fundamental frequency, which indicates that they contain contributions from both first harmonic modes and slow-varying modes, and might imply energy transfer between them.

Figure 3 compares the raw flow field with the reconstruction of the coherent velocity $\mathbf{u}_c$, with the 9 chosen FIR-SPOD modes and the mean velocity field. The frame is chosen at $t = 4.88$, which is around 1.6π of the shedding phase, when the streamwise rib structure is most easily observed in the flow. The structures are visualized by Q=0 isosurfaces colored by streamwise vorticity (Haller, 2005). $\mathbf{u}_c$ recovers 47% TKE and 69% Reynolds stress $\overline{u'v'}$ of the flow, and captures the coherent structures. The spanwise inhomogeneity of the von Kárman vortices, observed as the alternating streamwise vorticity and the changing local curvature, results from the perturbation due to 3D instabilities originating from interaction between the primary vortices and the rib-like streamwise vortices.

Above the diagonal of Figure 4, the phase portraits of the nine FIR-SPOD modes are shown, revealing temporal correlations through identifiable patterns. Circular trajectories in (a_1, a_2), (s_2, s_3), and (a_3, a_4) indicate coupled oscillatory modes with equal frequencies and quarter-phase shifts. The Lissajous curve between the first and second harmonic modes indicates the quadratic relationship in frequency with a phase offset. The paraboloid between the slow varying mode s_1 and a_1, a_2 verifies the nonlinear correlation $s_1 \propto \sqrt{a_1^2 + a_2^2}$. The paraboloid shown between s_8 and a_1, a_2, as well as the recognizable pattern between s_1 and s_8 solidify the claim that s_8 is part of the same coherent motion.

Below the diagonal of Figure 4, the temporal correlation among the temporal modes as the Galerkin system solution from equation (5) with initial eddy viscosity ν_T° computed in equation (6) is displayed. The Galerkin solution exhibits temporal correlation patterns consistent with the FIR-SPOD modes, indicating that the ROM successfully reproduces the temporal dynamics of captured coherent motions. For example, the circular trajectory between a_1 and a_2 is associated with the traveling instability, in this case the Kárman vortex shedding. The limit cycle observed between (s_2, s_3), (a_1, a_2) and

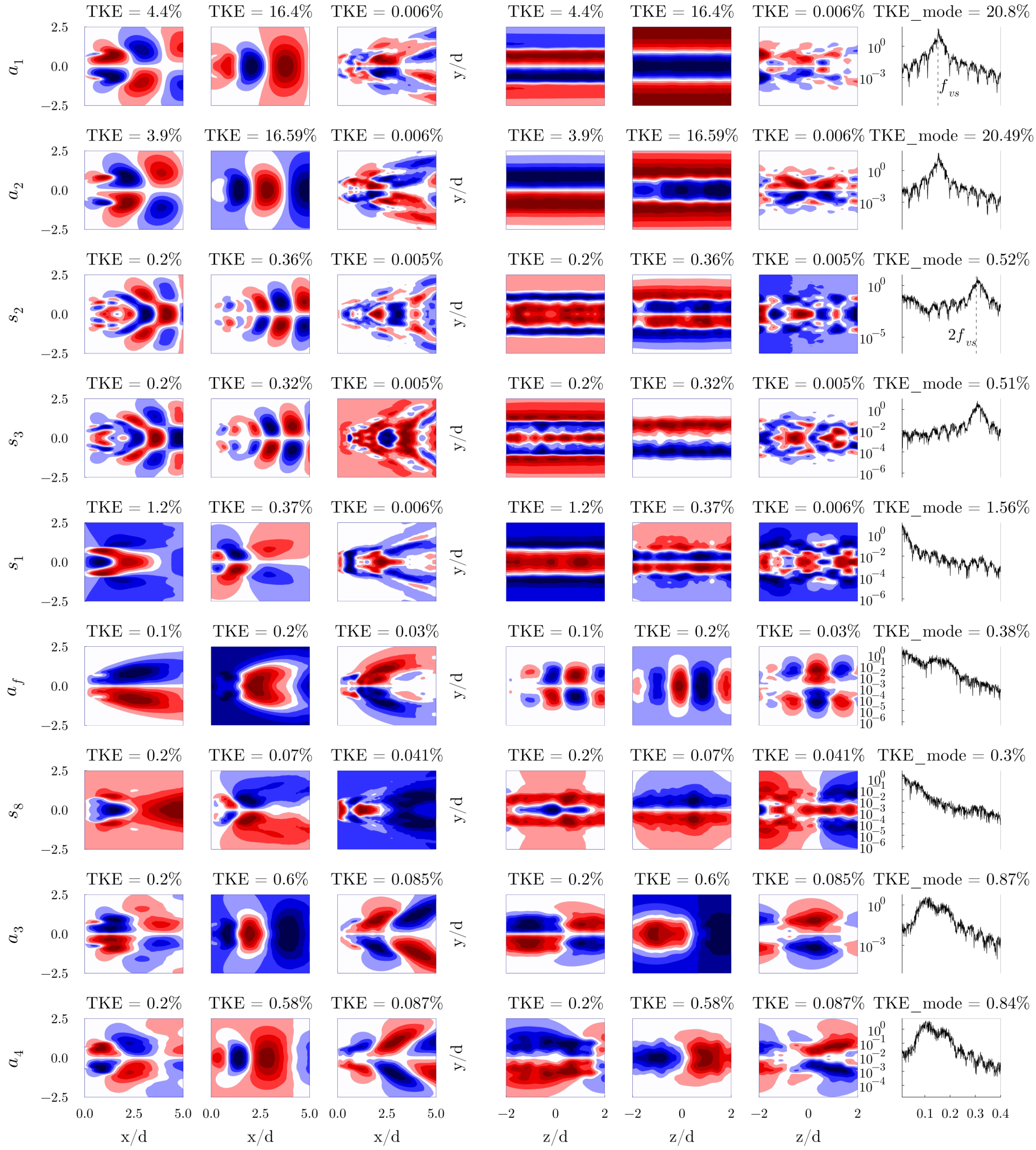

Figure 2: The 2D spatial profiles at $z = 0$ and $x = 0$ and temporal spectrum of nine chosen FIR-SPOD modes.

(a_3, a_4) implies the energy is redistributed between harmonic frequencies. A closer inspection shows that s_1, a_f and s_8, which relate to the slow varying motion, are coupled with the harmonic modes (a_1, a_2) and (s_2, s_3). This ROM highlights the interactions transferring energy between different motions.

CONCLUSION

In this study, a nonlinear system identification framework is developed and applied to the flow over the thin flat plate at a fully turbulent state. FIR-SPOD with a filter length of two shedding cycles is firstly utilized to capture the coherent motions from the velocity fluctuation: the primary vortices, the breathing motion in the wake, and the induction and partial occurrence of the rib-like streamwise vortices. A ROM describing the temporal evolution of the nine chosen interpretable FIR-SPOD modes is built through Galerkin projection. The dissipation and the Reynold stress contribution due to the truncated modes are modeled as a diffusion term through the eddy viscosity. The turbulent eddy viscosity is modeled as a function of the instantaneous kinetic energy from the resolved modes. The resulting Galerkin solutions capture the same intrinsic relationship among modes as the corresponding FIR-SPOD modes. The correlation observed in the Galerkin system solution validates the nonlinear modeling, and the nonzero nonlinear coefficients imply the irreversible energy transfer between scales.

In future work, the eddy viscosity will be optimized using the adjoint variable defined in equation (8). After extending the reconstructed system to the kinetic energy equation (12), the nonzero nonlinear coefficients representing the internal energy transfer and governing the triple correlation term will be investigated.

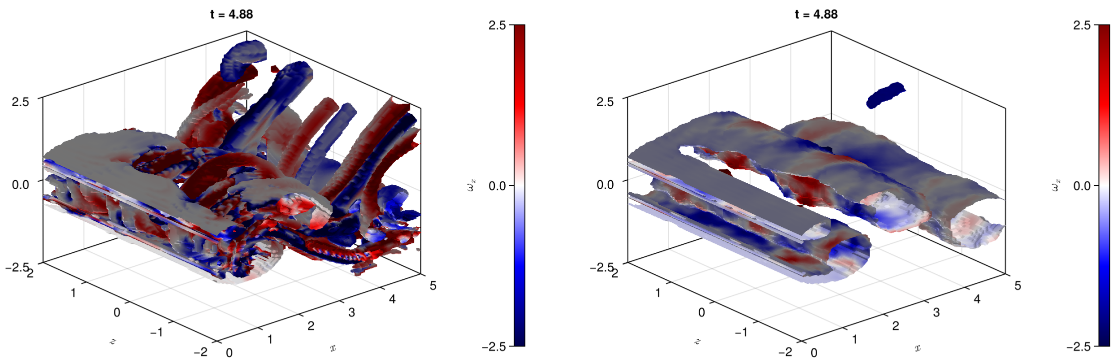

(a) data **u** colored by ω_x

(b) $\mathbf{u}^c$ colored by ω_x

Figure 3: The Q criterion of data and the reconstructed coherent motions at $t = 4.88$ colored by ω_x to show the capture of the induction and part occurrence of the streamwise ribs .

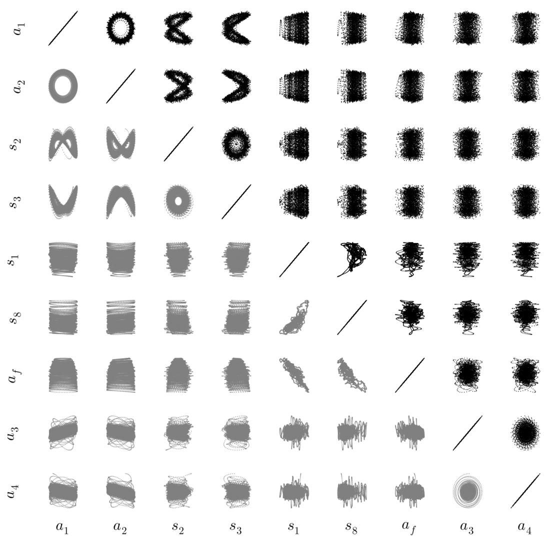

Figure 4: Phase portrait among Galerkin system solutions (gray dots and below the diagonal) and the FIR-SPOD modes (black dots and above the diagonal).

REFERENCES

Aubry, N., Holmes, P. & Lumley, J. L. et al. 1988 The dynamics of coherent structures in the wall region of a turbulent boundary layer. *J. Fluid Mech.* **192**, 115–173.

Ausseur, J., Pinier, J. & Glauser, M. et al. 2006 *Experimental Development of a Reduced Order Model for Flow Separation Control*.

Berkooz, G, Holmes, P & Lumley, J. L. 1993 The proper orthogonal decomposition in the analysis of turbulent flows. *Annu. Rev. Fluid Mech.* **25**, 539–575.

Brent, Richard P 1973 *Algorithms for Minimization Without Derivatives*. Englewood Cliffs, New Jersey: Prentice-Hall.

Haller, G. 2005 An objective definition of a vortex. *J. Fluid Mech.* **525**, 1–26.

Holmes, P., Lumley, J. L. & Berkooz, G. 1996 *Turbulence, Coherent Structures, Dynamical Systems and Symmetry*. Cambridge University Press.

Liu, D C & Nocedal, J. 1989 On the limited memory BFGS method for large scale optimization. *Math. Program.* **45**, 503–528.

Manohar, K. H., Williams, O., Martinuzzi, R. J. & Morton, C. 2023 Temporal super-resolution using smart sensors for turbulent separated flows. *Experiments in Fluids* **64** (5).

Noack, B. R., Afanasiev, K. & Morzynski, M. et al. 2003 A hierarchy of low-dimensional models for the transient and post-transient cylinder wake. *J. Fluid Mech.* **497**, 335–363.

Noack, B. R., Morzynski, M. & Tadmor, G. 2011 *Reduced-order modelling for flow control*, 2011th edn. Vienna, Austria: Springer.

Noack, B. R., Papas, P. & Monkewitz, P. A. 2005 The need for a pressure-term representation in empirical Galerkin models of incompressible shear flows. *J. Fluid Mech.* **523**, 339–365.

Oberleithner, K., Sieber, M. & Nayeri, C. N. et al. 2011 Three-dimensional coherent structures in a swirling jet undergoing vortex breakdown: stability analysis and empirical mode construction. *J. Fluid Mech.* **679**, 383–414.

Plessix, R.-E. 2006 A review of the adjoint-state method for computing the gradient of a functional with geophysical applications. *Geophysical Journal International* **167** (2), 495–503.

Protas, B., Noack, B. R. & Östh, J. 2015 Optimal nonlinear eddy viscosity in galerkin models of turbulent flows. *J. Fluid Mech.* **766**, 337–367.

Rosin, I. T. 2025 Fully turbulent wakes at low reynolds numbers: the case of the thin flat plate. *Master's thesis, University of Calgary, Calgary, Canada* .

Sieber, M., Paschereit, C. O. & Oberleithner, K. 2016 Spectral proper orthogonal decomposition. *J. Fluid Mech.* **792**, 798–828.

Tennekes, H. & Lumley, J. L. 1972 In *A First Course in Turbulence*. The MIT Press.

Thompson, M. C., Radi, A. & Rao, A. et al. 2014 Low-reynolds-number wakes of elliptical cylinders: from the circular cylinder to the normal flat plate. *J. Fluid Mech.* **751**, 570–600.

Towne, A., Schmidt, O. T. & Colonius, T. 2018 Spectral proper orthogonal decomposition and its relationship to dynamic mode decomposition and resolvent analysis. *J. Fluid Mech.* **847**, 821–867.

Williamson, C H K 1996 Vortex dynamics in the cylinder wake. *Annual Review of Fluid Mechanics* **28**, 477–539.

Östh, J., Noack, B. R. & Krajnović, S. et al. 2014 On the need for a nonlinear subscale turbulence term in pod models as exemplified for a high-reynolds-number flow over an ahmed body. *J. Fluid Mech.* **747**, 518–544.